Cell Reports
Physical Science

CellPress
OPEN ACCESS

Article

Implantation-assistance-free flexible waveguide probe for optogenetic stimulation

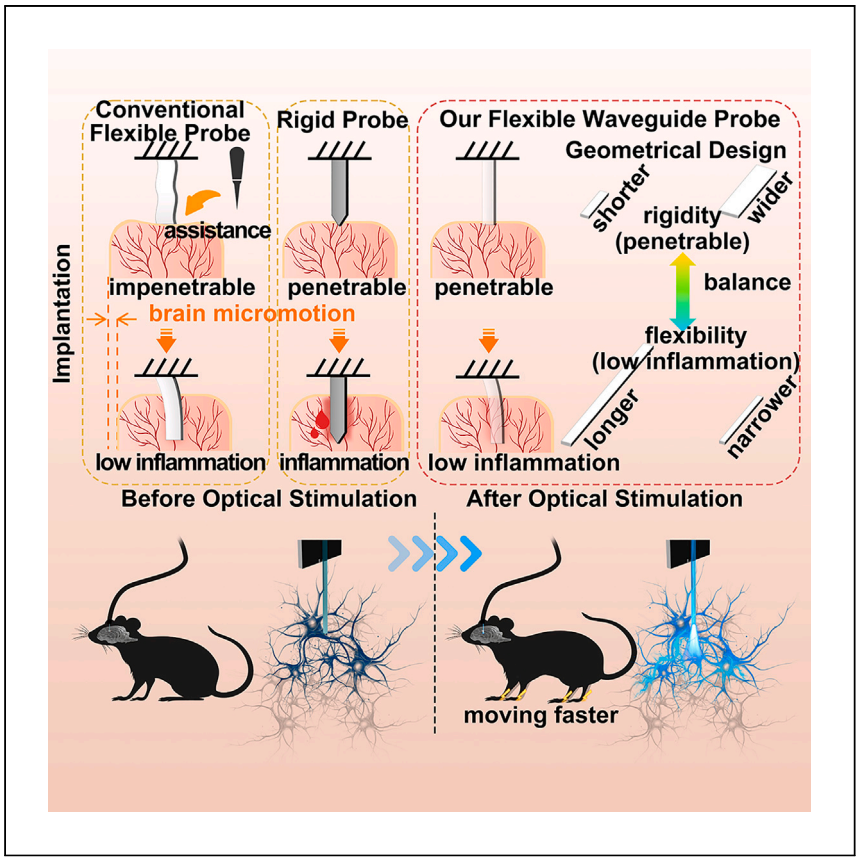

Chen et al. propose the optogenetic waveguide probe for brain modulation. The probe strikes a delicate balance between flexibility, inherent to the characteristics of polymers, and rigidity through its meticulous geometrical design, which can help achieve direct, precise, and deep implantation.

Zequn Chen, Xiaojing Li, Yiheng Tang, ..., Ke Si, Wei Gong, Lan Li

jianghanqing@westlake.edu.cn (H.J.)
kesi@zju.edu.cn (K.S.)
weigong@zju.edu.cn (W.G.)
lilan@westlake.edu.cn (L.L.)

Highlights

Precise, deep, and low-damage probe implantation in the mouse brain

Optimized optical and mechanical design to facilitate assistance-free implantation

Minimized motion artifacts and inflammatory response in chronic bio-experiments

Effective behavior modulation of the mouse by flexible waveguide optogenetic probe

Chen et al., Cell Reports Physical Science 5, 102217
October 16, 2024
Published by Elsevier Inc.
https://doi.org/10.1016/j.xcrp.2024.102217

Cell Reports
Physical Science

CellPress
OPEN ACCESS

Article

Implantation-assistance-free flexible waveguide probe for optogenetic stimulation

Zequn Chen,[1,2,11] Xiaojing Li,[3,4,11] Yiheng Tang,[1,2,11] Zhanchao Huang,[2,5,11] Ji Huang,[1,2] Haoran Liu,[6] Yang Weng,[1,2] Yue Zhu,[7] Jingyang Zhao,[2,5] Renjie Tang,[1,2] Zhu Liu,[6] Kangjian Bao,[1,2] Jialing Jian,[1,2] Yuting Ye,[1,2] Yiting Yun,[8] Lichun Wang,[8] Chengchen Guo,[5,6,9] Hongtao Lin,[3,8] Hanqing Jiang,[2,5,*] Ke Si,[3,4,7,*] Wei Gong,[3,4,*] and Lan Li[1,2,9,10,12,*]

SUMMARY

The optogenetic probe has proven to be a valuable tool in neuroscience, owing to its specific stimulus properties. Mechanically flexible optogenetic probes are crucial for chronic and deep brain stimulation, minimizing tissue damage, and improving long-term stability and reliability. However, the current implantation of flexible polymer probes often requires the use of additional auxiliary tools, which complicate the surgical process and may cause severe inflammatory responses. In this paper, we propose a flexible polymer waveguide optogenetic probe designed to be inserted directly and precisely into the target brain area without additional assistance through geometric and mechanical optimization of the probe. It also exhibits superior long-term performance in minimizing the inflammatory response after implantation. We eventually succeed in modulating mouse locomotor speed by brain secondary motor cortex (M2) stimulation. This study provides a reference for the future development of flexible waveguide optogenetic probes for reliable and long-term implantation.

INTRODUCTION

The comprehension of brain function and the therapeutic management of neurological disorders highly hinge upon the ongoing development of sophisticated methodologies to interrogate the intricate workings of the nervous system.[1–5] In recent decades, optogenetic techniques have emerged as potent instruments for precise and efficacious neural modulation owing to their capacity for cell-specific targeting.[6–8] For manipulating the activity of specific neurons or neuronal circuits in deep brain regions, silica optical fibers[9,10] serve as the commonly used optogenetic probes. However, the average Young's modulus of silica optical fibers is at least five or six orders of magnitude greater than that of neuronal tissues.[9,11] The significant elastic mismatch can damage the native tissue, leading to severe inflammatory responses in the brain and neuronal apoptosis in the implanted area.[12,13] To address this problem, stretchable and flexible optoelectronic probes[8,14–18] and polymer waveguide probes[19–23] have been developed with reduced tissue inflammation and sustained stability in the probe performance for chronic implantation. Nonetheless, the intricate and costly manufacturing process of implantable optoelectronic devices, coupled with the challenges of precise, deep, and low-damage implantation in the brain inherent in flexible polymer (such as Parylene,[23] hydrogel,[20,24,25]

[1]Key Laboratory of 3D Micro/Nano Fabrication and Characterization of Zhejiang Province, School of Engineering, Westlake University, Hangzhou, Zhejiang 310030, China

[2]Institute of Advanced Technology, Westlake Institute for Advanced Study, Hangzhou, Zhejiang 310024, China

[3]MOE Frontier Science Center for Brain Science & Brain-Machine Integration, Zhejiang University, Hangzhou, Zhejiang 310027, China

[4]NHC and CAMS Key Laboratory of Medical Neurobiology, School of Brain Science and Brain Medicine, Zhejiang University, Hangzhou, Zhejiang 310058, China

[5]Research Center for Industries of the Future, School of Engineering, Westlake University, Hangzhou, Zhejiang 310030, China

[6]School of Engineering, Westlake University, Hangzhou, Zhejiang 310030, China

[7]State Key Laboratory of Modern Optical Instrumentation, College of Optical Science and Engineering, Zhejiang University, Hangzhou, Zhejiang 310027, China

[8]Key Laboratory of Micro-Nano Electronics and Smart System of Zhejiang Province, College of Information Science and Electronic Engineering, Zhejiang University, Hangzhou, Zhejiang 310027, China

[9]Westlake Laboratory of Life Sciences and Biomedicine, Hangzhou, Zhejiang 310024, China

[10]Westlake Institute for Optoelectronics, Westlake University, Fuyang, Zhejiang 311421, China

[11]These authors contributed equally

[12]Lead contact

*Correspondence:
jianghanqing@westlake.edu.cn (H.J.),
kesi@zju.edu.cn (K.S.),
weigong@zju.edu.cn (W.G.),
lilan@westlake.edu.cn (L.L.)

https://doi.org/10.1016/j.xcrp.2024.102217

and polymethylhydrosiloxane (PDMS)[26,27]) probes, have impeded their widespread adoption in practical applications.

Recently, SU-8, a commonly used epoxy-based polymer with low propagation loss in the visible spectrum,[28] has emerged as a prominent material candidate for optogenetic waveguide-integrated probes.[29,30] The flexible probe based on SU-8 showed the exceptional feature of scar-free integration with tissues due to its inherent flexibility with a lower Young's modulus,[31] along with its advantageous characteristics in experimental studies, such as reduced inflammation response, which has been consistently corroborated in experimental investigations within the realm of flexible electronics.[31] Despite this, the feasibility and potential merits of using SU-8 as flexible, low-loss waveguide probes for optogenetic brain modulation in animals have not been thoroughly investigated.

In this study, we develop a simplified approach to constructing a flexible and durable waveguide probe based on SU-8 for optogenetic modulation (Figure 1A), which overcomes the fabrication complexity and implantation challenge of conventional flexible probes. To simplify the implantation procedure, we establish a flexible waveguide probe implantation model without additional guiding fixtures by optimizing the geometric structure of the probe profiles with mechanical analysis (Figure 1B). The structurally optimized flexible probes can be directly implanted under the condition that the critical buckling force (F_{cb}) of the flexible probe is greater than the critical penetration force (F_{cp}), significantly improving the implantation precision and reducing the complexity of the surgery. Additionally, mechanical simulation and bio-experiment results demonstrate that the use of flexible probes effectively decreases tissue inflammation following acute and long-term (4-month) periods in comparison to rigid probes due to the reduced interaction between the adjacent brain tissue and flexible probes during minor brain tissue micromotion. We then implant the flexible waveguide probe into the secondary motor cortex (M2) of the mice and successfully modulate their locomotor speed by delivering stimulation light (Figure 1C), indicating its operational reliability. This approach presents a design protocol that offers a paradigm for designing upcoming optoelectronic devices and a prototype of flexible waveguide-integrated optogenetic probes that could provide a benchmark for future optical human-machine interfaces.

RESULTS

Optical characterization of the SU-8 waveguide

The low transmission loss of the waveguide improves the optical transmission efficiency, stability, and system performance of the device. Therefore, before preparing the flexible waveguide probe, we first optimized the lithography process of the SU-8 waveguide to reduce the waveguide pattern roughness, which is the key to propagation loss. Sidewall and cross-section images of the waveguide prepared by photolithography are shown in Figures S1A and S1B, showing the smooth and straight wall, which favors the reduction of the propagation loss. Subsequently, we measured the optical propagation loss of waveguides at different wavelengths using the cut-back method. The corresponding schematic diagram of the waveguide propagation loss measurement setup is shown in Figures S2–S4. Waveguides have been found to exhibit low loss propagation throughout the entire visible spectral range, which is attributed to their high transmission in this range, as shown in Figure 2A. This feature makes them a promising candidate for serving as a dual-color or even multicolor light emitter, allowing them to switch between excitation and inhibition modes during neuronal modulation.[7,32] The results of the optical propagation loss

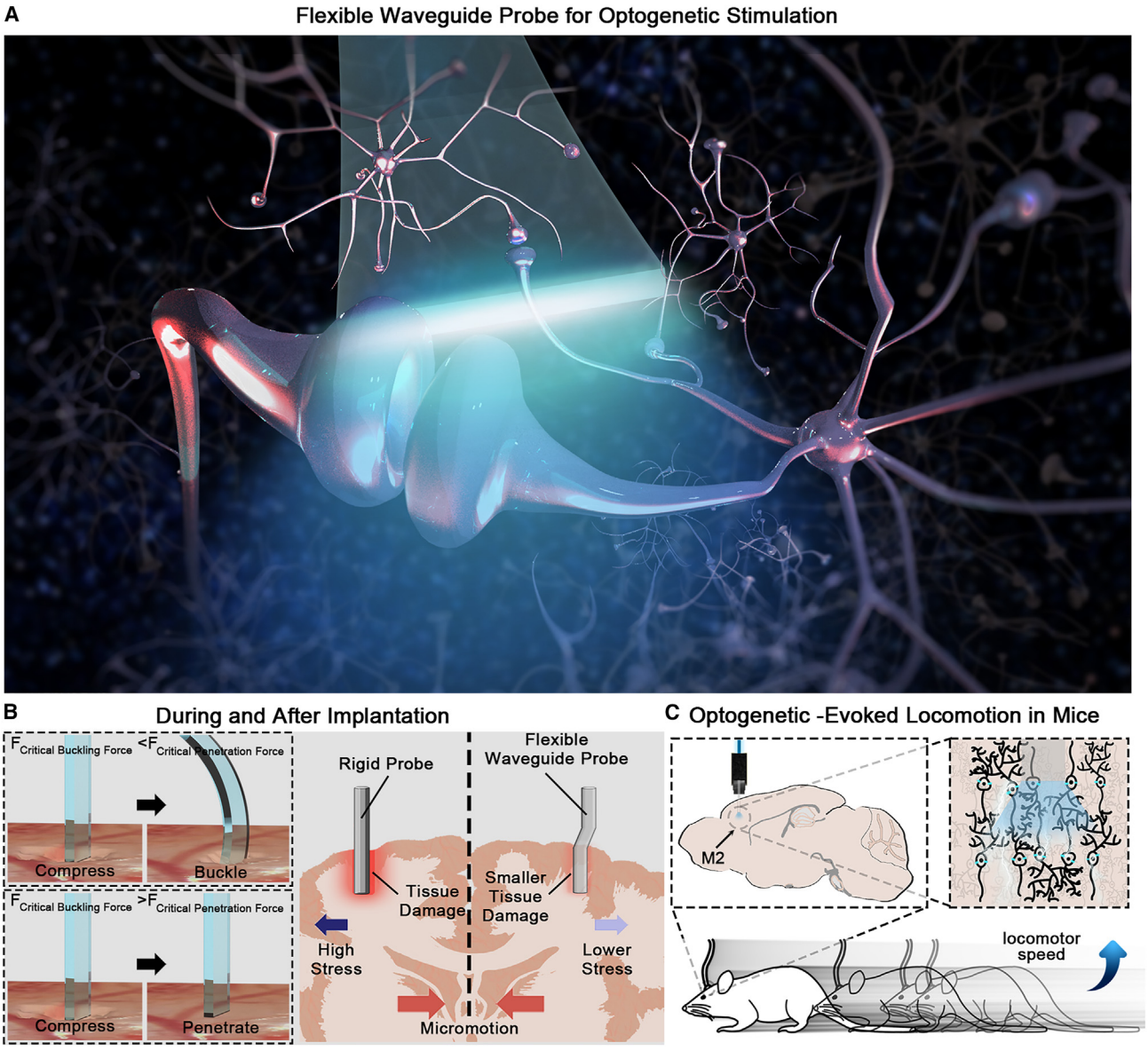

Figure 1. Conceptual illustration of a flexible waveguide probe with direct implantation capability and low tissue damage for optogenetic neural activity modulation

(A) Conceptual diagram of flexible waveguide optogenetic probes for neuronal modulation.

(B) Schematic representation of the mechanical scenario at the surface of brain tissue faced by the flexible probe during implantation (left) and schematic representation of the state of the flexible waveguide probe compared to the rigid probe in the brain tissue after implantation (right).

(C) Schematic illustration of the elevation of locomotor speed in mice caused by probe stimulation of neurons in the M2 brain region expressing the corresponding photosensitive proteins.

measurements of the SU-8 waveguide at 473, 532, 589, and 633 nm are illustrated in Figures 2B and S1C–S1F and Note S1, respectively. The waveguide presents optical propagation losses of 4.25 $\pm$ 0.19 dB/cm at 473 nm, 3.61 $\pm$ 0.09 dB/cm at 532 nm, 2.80 $\pm$ 0.01 dB/cm at 589 nm, and 2.43 $\pm$ 0.07 dB/cm at 633 nm, showing a superior propagation loss to that of flexible Parylene C waveguides[23,33] and other materials, like silicon nitride (Si_3N_4)[34,35] and titanium dioxide (TiO_2),[35,36] as compared in Table S1. From the perspective of the working wavelength, the SU-8 waveguide demonstrates a relatively low propagation loss within the 470–650 nm range, with

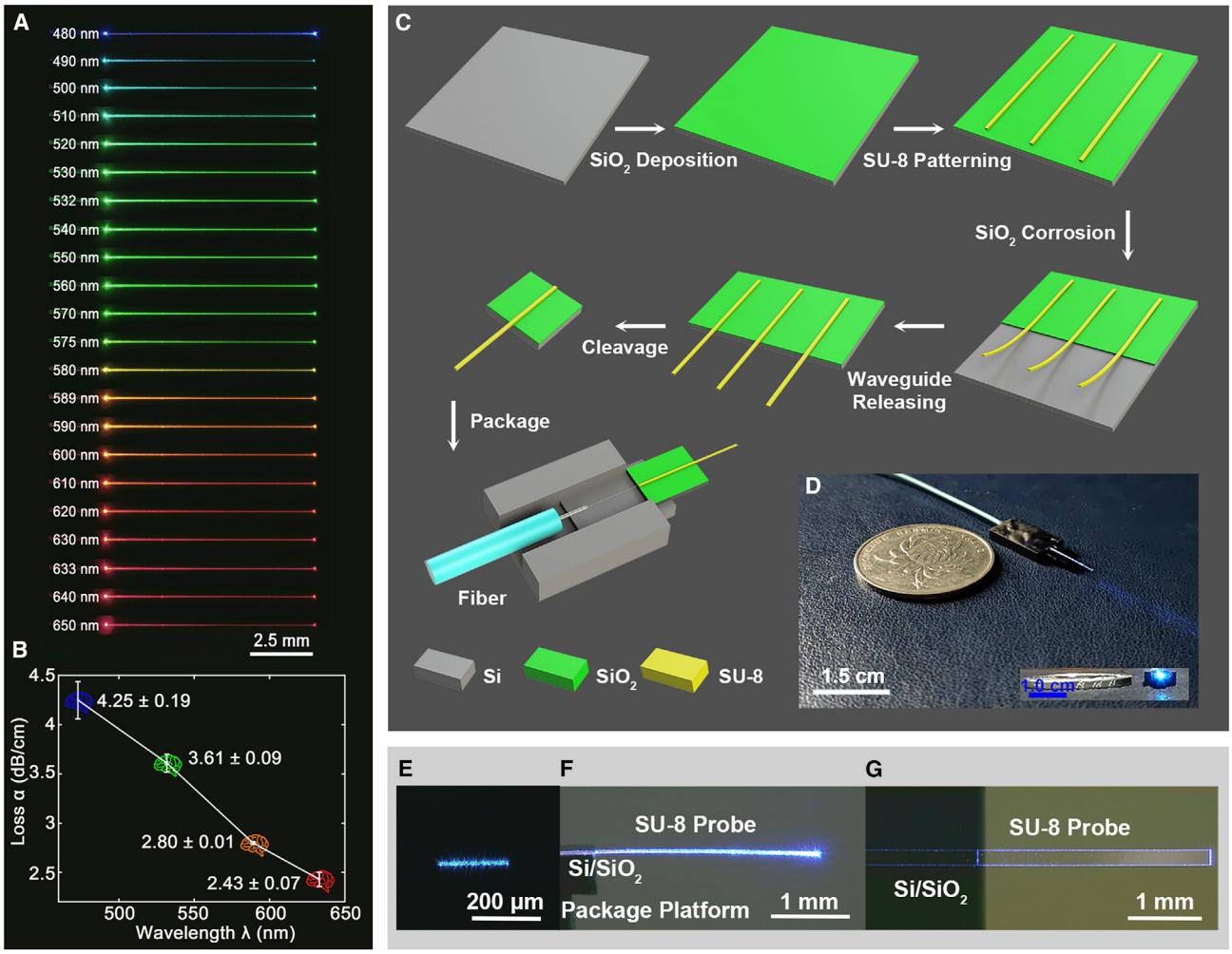

Figure 2. Fabrication and optical performance characterization of flexible waveguide probe

(A) Side-view dark-field images of the waveguide at different λ (scale bar, 2.5 mm).

(B) Measured optical waveguide propagation loss at the wavelength of 473, 532, 589, and 633 nm. Data are represented as mean ± standard deviation. The error bars originate from multiple tests over 5 samples.

(C) Fabrication process diagram of the flexible waveguide probe.

(D) Photo image of a well-encapsulated flexible waveguide probe (scale bar, 1.5 cm). The inset shows a cross-section of the probe (scale bar, 1 cm).

(E–G) The digital photographs of a free-standing waveguide probe: (E) cross-section view (scale bar, 200 μm), (F) side view (scale bar, 1 mm), and (G) top view (scale bar, 1 mm).

its additional biocompatibility making it suitable for optogenetic applications in the visible spectral range.

Fabrication and encapsulation of flexible waveguide probes for optogenetic stimulation

Leveraging its appropriate optical performance, we further developed the SU-8 waveguide into a flexible optogenetic stimulation probe. Compared with its rigid counterpart (SU-8 waveguide on a rigid silicon shank; Note S2; Figure S5), our demonstrated flexible waveguide probes exhibit superior benefits in the fabrication process, mechanical stability, and biocompatibility. Explicitly speaking, flexible probe technology can be achieved with a reduced number of steps in the manufacturing procedures and fewer technical difficulties, highly improved experimental efficiency, and reduced costs. Figure 2C reveals the preparation process

diagram of the flexible probes. The details of the fabrication process are shown in Note S3. Waveguides are fabricated on oxide using UV photolithography. We employed a combination of hydrofluoric acid (HF) wet etching and dissociation to release flexible probes as an alternative to the conventional back silicon etching approach, thereby reducing the number of process steps and the complexity. For optical packaging, the scheme of a conventional optical fiber for rigid silicon probes uses a U-groove.[29] However, after probe implantation, the adhesion between the bare fibers and the chip was susceptible to breakage due to the pulling force exerted during mouse movement, as illustrated in Figure S6. To resolve this issue, we developed an original encapsulation protocol to improve the mechanical stability of the probe system after the implantation procedure, as shown in Figure 2C. Through three-dimensional (3D) printing technology, a groove-shaped polymer platform was printed, and a probe chip was fixed to the platform's front end. The optical fiber was connected to the probe through an alignment platform (Figure S7), and its connection was reinforced with an adhesive. An image of a well-encapsulated flexible waveguide probe is shown in Figure 2D. Thus, when the mouse moved, the generated force was loaded to the whole packaging platform rather than the adhesion area of the optical fiber to the chip (Figure S6), ensuring the robustness of the implanted probe throughout the mouse's movements. In contrast to recently reported polymer-based optogenetic probes such as Parylene C,[23,33,37] our flexible SU-8 waveguide probes stand out for their convenient fabrication process. Compared to hydrogel, which is frequently used to prepare flexible optical fibers,[19,24,25,38] SU-8 has superior and long-term stability in liquid environments, such as brain tissue. When the polymer probe is released into a free-standing state, severe deflection usually occurs at the tip of the flexible probe. This indicates that the probe is excessively flexible and unable to bear its weight, potentially limiting its ability to reach the target area[31,39] through the stereotaxic surgery platform. In contrast, Figures 2E–2G and S8 display the flexible suspended waveguide in probes with light delivery. We observed that the released flexible probes exhibit nearly imperceptible deflection in the horizontal direction. This behavior can be attributed to the structurally optimized probe's suitable flexural stiffness, which is essential for precise and direct implantation, eliminating the necessity for rigid guiding fixtures.[37,40] When the laser individually emitted 1 mW light at the wavelength of 473 nm, the output optical power density of the waveguide probe was 43.3 mW/mm^2, which exceeded the thresholds for optogenetic stimulation of channelrhodopsin-2 (ChR2) opsin (1 mW/mm^2),[41] indicating our outstanding and well-packaged encapsulation technology.

Design and analysis of flexible waveguide probes for assistance-free implantation

Owing to the inherent flexibility of polymers, implanting polymer-based flexible probes in biological tissues directly, without external assistance, poses challenges for surgical operators. In terms of insertion, assistance-free implantation of the flexible probe must address the primary issues of maintaining elastic stability and preventing buckling during insertion. This necessitates direct implantation theory (DIT), which posits that a flexible probe must have an F_{cb} greater than the F_{cp} to ensure successful and safe implantation. First, we performed a finite element analysis (FEA) to quantitatively evaluate the mechanical behaviors of SU-8, silicon, and silica optical fiber probes, respectively (see Note S4 for details). The von Mises stress, which is an effective indicator for predicting the yielding and failure of materials under loading, is presented in Figure 3A for the three probes at the point of buckling. In the coordinate system shown in the figure and used in this study, the y axis aligns with the length of the probe, the z axis with its width, and the x axis

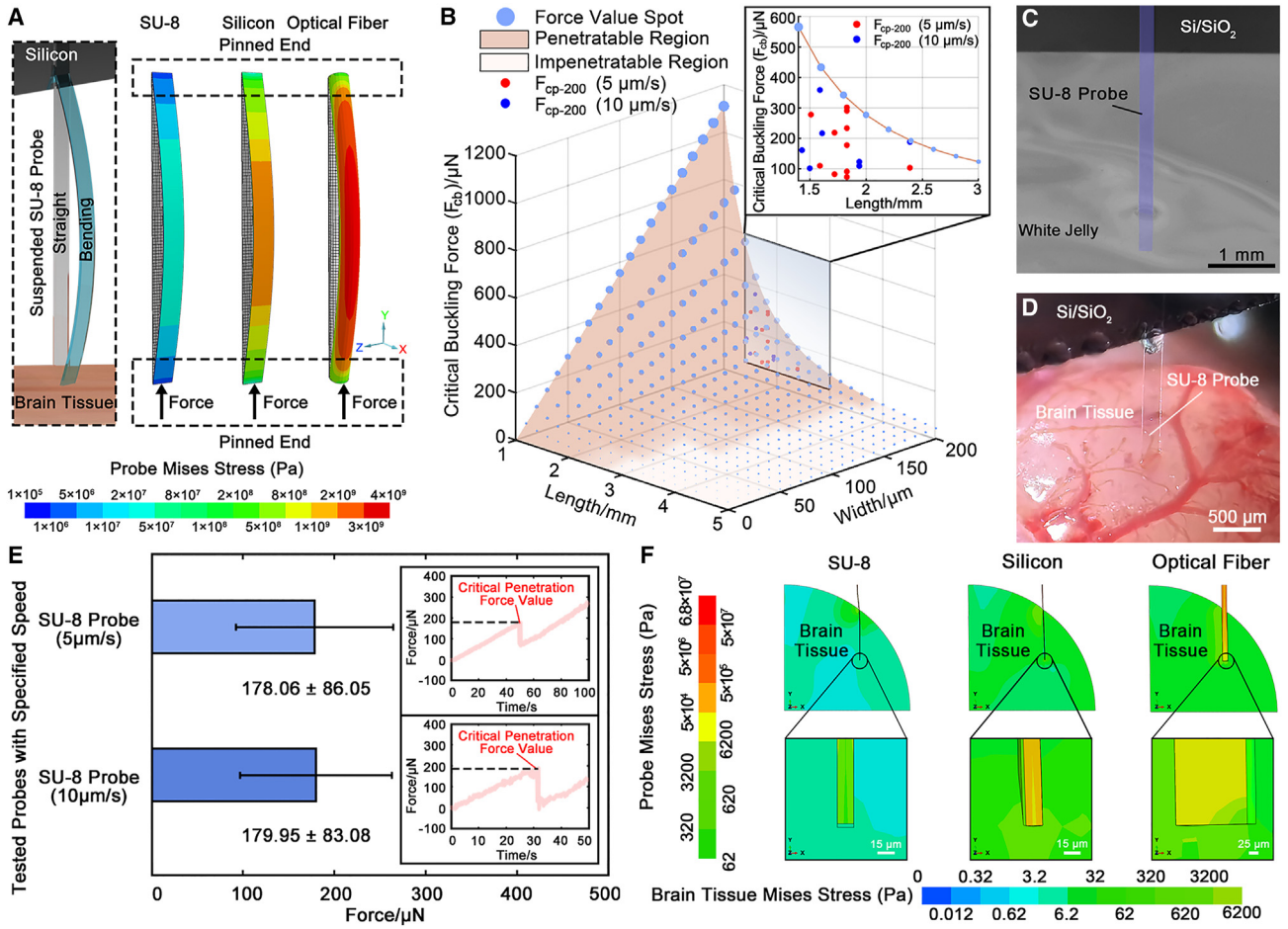

Figure 3. Mechanical analysis of flexible waveguide probes during implantation and probe-tissue interactions under brain micromotion

(A) Simulation of von Mises stress at buckling for probes made of flexible SU-8, rigid silicon, and silica optical fiber. The bends (or buckles) of the probes occur along the y axis direction.

(B) Experimentally obtained and calculated the critical bucking force of flexible waveguide probes with different lengths and widths. The light blue dots represent the theoretical calculation of the critical buckling force. The dark shaded and light shaded regions indicate the dimensions of the implantable/non-implantable probes verified through implantation surgery. The inserted plot demonstrates the calculated F_{cb} in comparison with the measured F_{cp} at implantation velocities of 5 (red dot) and 10 μm/s (blue dot) for flexible waveguide probes with a width of 200 μm and various lengths.

(C and D) Insertion of the flexible waveguide probe into the phantom brain (white jelly with matching Young's modulus of the mouse's brain) (scale bar, 1 mm) (C) and actual brain tissue (scale bar, 500 μm) (D) of a male wild-type mouse under anesthesia.

(E) Comparison of the collected F_{cp} for flexible waveguide probes with different implantation speeds. The inset is the F_{cp} curve of the flexible waveguide probe at implantation velocities of 5 and 10 μm/s, respectively. Data are represented as mean ± standard deviation. The error bars are derived from multiple tests (5 μm/s) over 11 samples and 7 samples (10 μm/s), respectively.

(F) Simulated von Mises stress profiles within the brain tissue for probes based on flexible SU-8, rigid silicon, and silica optical fiber under 100 μm lateral micromotion (along the x axis direction) of the brain tissue. The interaction force mainly exerts on the z-y plane of the probes. Scale bars in three enlarged diagrams of the probe tips represent 15, 15, and 25 μm.

with its thickness. Compared with the rigid bare silicon (without the SU-8 waveguide on silicon) and the silica optical fiber probe, the SU-8 buckled at a much smaller stress level (at least two orders of magnitude smaller), indicating that the flexible probe was more prone to bending than the rigid probe. However, the negligible deflection under its weight (as shown in Figure 2F) suggests that the flexible waveguide probe can be stable enough to achieve implantation without any guiding fixture. To ensure that the probe withstands the forces exerted on it during implantation without buckling or failure, F_{cb} should exceed F_{cp}. Thus, we first illustrated the effect of the size of the flexible probe on its F_{cb} and insertion through theoretical

calculations using both Euler-Bernoulli beam theory and implantation experimentation. The details are discussed and shown in Note S5. As shown in Figure 3B, with the elongation of the flexible probe and the reduction in its width, there is a gradual decrease in the F_{cb} (light blue dots) of the flexible probe, rendering its unassisted implantation more challenging (the light shaded region), as verified through implantation surgery. While shorter and wider probes demonstrate relatively higher F_{cb} and can be implanted smoothly into the brain tissue (the dark shaded region) without any guiding fixture, they impede deep brain stimulation owing to their limited insertion depth. Therefore, the trade-off between the probe insertion conditions and operational requirements was carefully considered to ensure the functionality and utility of the probes. The direct implantation experiment of a flexible waveguide probe without assistance was successfully demonstrated in both a phantom brain and a real mouse brain, as shown in Figures 3C, 3D, and S9 and Video S1.

We also considered the effect of the speed at which the probe was inserted during implantation (Figure 3E). The inset of Figure 3E shows the mechanical test curve of the penetration force at the tip of the flexible waveguide probe at the time of implantation at different insertion speeds. The sudden drop in the curve signifies the penetration of the flexible probe into the brain tissue. Hence, the force value corresponding to the point of this sudden drop represents F_{cp} (see Note S6 for details). We found that the influence of the needle insertion speed on F_{cp} at the current scale was negligible (Figure 3E). There must be a strong correlation between the penetration force and other factors, such as the probe type, animal species, age, and target tissue area.[42] To verify DIT, we compared the F_{cp} measured by flexible waveguide probes of different lengths with their corresponding F_{cb}, as indicated in the inset of Figure 3B. The F_{cp} of probes shorter than 2.5 mm was found to be below their corresponding F_{cb}, suggesting that these probe lengths are suitable for direct implantation in mouse brains, providing quantitative validation for the implantation experiment. If both conditions (negligible deflection of flexible probes and $F_{cb} > F_{cp}$ during implantation) are simultaneously met, the risk of buckling during insertion can be avoided, thereby achieving implantation without requiring external auxiliary methods. Our findings may predict the probability of successful implantation of an unknown-sized flexible probe system based on similar mechanical properties.

We further investigated the mechanical interactions between the biological tissue and flexible waveguide probes. Due to the planar geometry of the probe and the limited adhesive properties between SU-8 and biological tissue,[43] the predominant mechanical interaction between the probe and surrounding brain tissue is primarily governed by probe bending.[21,38] Therefore, the bending stiffness of the flexible waveguide probe is the key parameter for the interaction between tissues and probes.[38] In Figure S10, the characterized bending stiffness of the flexible SU-8 probe (2.1×10^{-2} N/m) is two orders of magnitude smaller than those of the silica optical fiber probe (8.6 N/m) and the rigid bare silicon probe (2.2 N/m) due to the lower Young's modulus of SU-8, making it a favorable choice for minimizing the biomechanical impact on surrounding brain tissue.[31,44] The details of the measurements are presented in Note S7. To study the mechanical interaction between implanted flexible waveguide probes and brain tissue, we developed a finite element model that simulates micromotion in the brain under physiological conditions (Figures 3F, S11, and S12; Note S8; Videos S2, S3, and S4). The section of the simulation model in Figure 3F is intercepted along the x direction, as shown in Figure S11. The numerical analysis demonstrates that a flexible waveguide probe with lower bending stiffness results in a lower stress level within the surrounding tissue during micromotion simulation compared to rigid bare silicon probes and silica optical

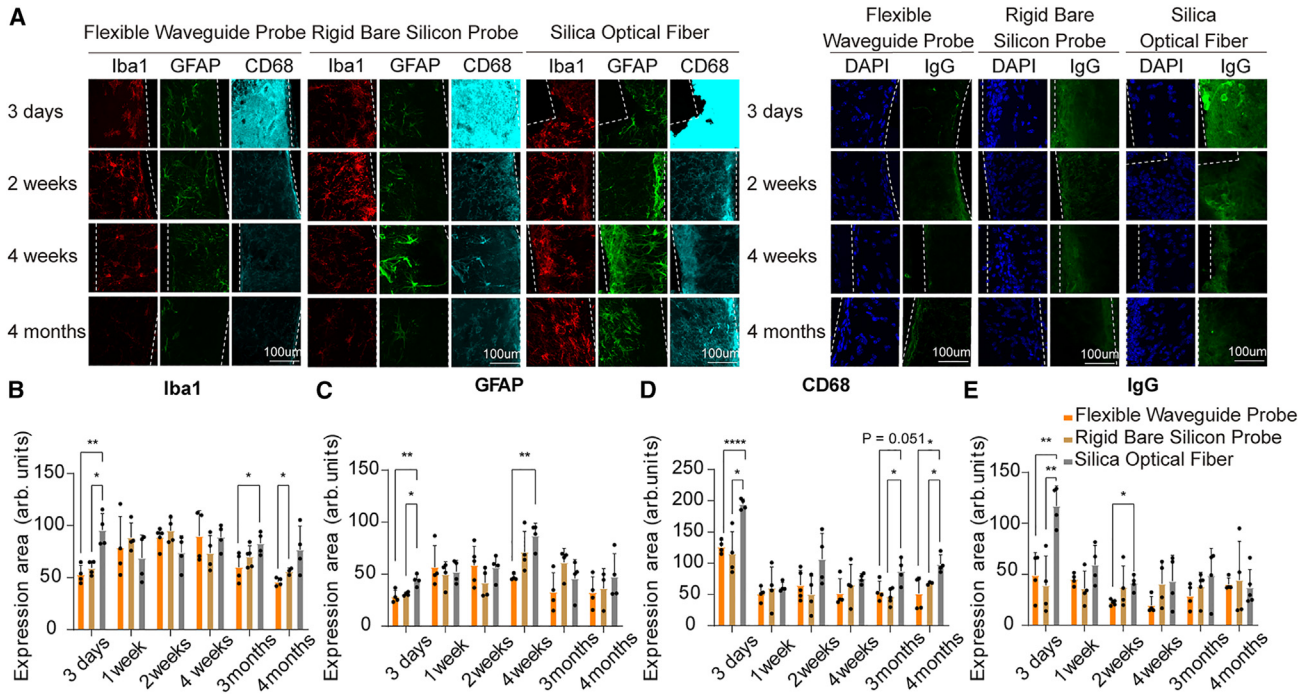

Figure 4. *In vivo* inflammation response comparative tests

(A) Immunohistochemical comparisons of tissue responses after probe implantation at different periods. Representative immunohistochemistry images tagged with Ibal (red), GFAP (green, left), CD68 (cyan), and Iba1 (green, right) in the vicinity of the flexible waveguide probes, rigid bare silicon probes, and commercial silica optical fibers for 3 days, 2 weeks, 4 weeks, and 4 months following the implantation, respectively (zoomed-in images, related to Figure S13). Cell nuclei were stained by 4′,6-diamidino-2-phenylindole (DAPI; blue). The white dashed lines indicate the contact boundary between the implanted probes in mouse brain tissues. All scale bars, 100 μm.

(B–E) Quantitative comparisons of mean immunofluorescence regions of Iba1 (B), GFAP (C), CD68 (D), and IgG (E) near flexible waveguide probes, rigid bare silicon probes, and a commercial silica optical fiber at 3 days, 1 week, 2 weeks, 4 weeks, 3 months, and 4 months after implantation. Two-way ANOVA with multiple comparisons correcting; for GFAP, $N = 4$ trials each duration of different probes; for IgG, $N = 4.17$ trials each duration of different probes. All the brain sections were collected from 36 male wild-type mice. *$p < 0.05$, **$p < 0.01$, and ****$p < 0.0001$.

fibers. Thus, the flexible waveguide probe can minimize shear damage resulting from brain micromotion.

In vivo inflammation response comparative tests with flexible/rigid probes

To further verify the low tissue damage of the flexible waveguide probe after implantation *in vivo*, we demonstrated the tissue inflammation response of the flexible waveguide probe, commonly used rigid bare silicon probes with nearly the same geometry and dimensions, and commercial silica optical fibers. The tissue inflammation response at different periods after implantation was evaluated through immunohistochemistry analysis of foreign body reactions, validating the advantage of the flexible probes in reducing tissue inflammation. A description of the experiments is provided in Note S12. To assess the foreign body response to the probes, we selected specific markers for analyzing their expressions at the implantation site of mouse brain tissues, as depicted in Figure 4A. Specifically, we employed astrocyte glial fibrillary acidic protein (GFAP) for identifying glial scarring, ionized calcium-binding receptor molecule 1 (Iba1) for labeling microglial cells, the cluster of differentiation 68 (CD68) for detecting macrophage activation, and immunoglobulin G (IgG) as a marker to assess blood-brain barrier integrity. After implantation of the probes into the mouse brain for durations of 3 days, 1 week, 2 weeks, 4 weeks, 3 months, and 4 months, the mouse brain tissues were collected for coronal

sectioning. The expression of the aforementioned marker proteins was labeled to compare the differences in tissue inflammation responses among the three types of implants using immunohistochemistry.

In the initial stage, the tissue reaction to the implanted probes is primarily influenced by the effects of insertion, such as acute tissue damage during the implantation process.[31,45] Over the long term, in contrast, the predominantly influential factor on tissue response is the chronic interaction between the tissue and the implants, specifically pertaining to factors such as micromotion.[46,47] Therefore, as shown in Figures 4B–4E, 3 days after implantation, the expression of biomarkers proximal to the flexible waveguide probe exhibited a marked reduction compared to that surrounding the silica optical fiber. Conversely, the tissue reaction to the rigid bare silicon probe resembled that of the flexible waveguide probe, owing to their analogous geometries. After a prolonged implantation time (1, 3, and 4 months), the flexible waveguide probe demonstrated a markedly diminished foreign body response in comparison to both the rigid bare silicon probe and the silica optical fiber (Figures 4B–4E), indicating the advantages of the flexible waveguide probe in reducing the inflammation of the foreign body reaction in brain tissue.

In vivo behavioral modulation experiment in mice

To validate the efficacy of the flexible SU-8 waveguide optogenetic system in rodent brain studies, we utilized a 473 nm wavelength laser to precisely stimulate the right M2 neurons of male Thy1-Cre transgenic mice expressing ChR2 (Figure 5A) to recreate the previous study on motion speed change behavior.[48] The details of the related behavioral experiments are described in Notes S9–S11 and S13–S15. We conducted post hoc histological validation to confirm M2 pyramidal neurons expressing ChR2, as presented in Figure 5B. Images of mice in the convalescent period after implantation surgery are shown in Figure 5C. Mice were placed individually in a cylindrical chamber to replicate the optogenetic experiment by the system, as illustrated in Figure S14. A controlled experimental step involving alternating epochs of 2 min blue light emission and 2 min periods without light emission was achieved through a signal generator. Video tracking software was used to monitor the locomotion of mice within the designated area. A control experiment was conducted to ensure the consistency of the stimulation parameters in mice using a 589 nm laser that operates within the non-sensitive range of ChR2. The results demonstrated that photostimulation of ChR2-expressing mice with blue light, but not yellow light, effectively increased their locomotor speed. Compared to the light-off epoch, the optogenetic system based on the flexible waveguide probe effectively realized a 10% increase in locomotor speed in ChR2-expressing mice (Figures 5D and 5E). These findings suggest that implantation of the flexible waveguide probe can successfully transmit visible light, enabling optogenetic perturbation of neurons in the motor cortex, indicating its efficacy. The effectiveness of optogenetic activation was further verified by c-Fos staining in the stimulated region, as illustrated in Figures 5F–5H and S15. Photoactivation of the M2 region using the flexible waveguide probe validates its optogenetic efficacy and refines the procedure of probe implantation and bio-experimental testing.

DISCUSSION

In this study, we present a flexible waveguide probe that obviates the need for supplementary external auxiliary implantation for optogenetic stimulation in mice's brains. The implantation model was optimized by refining the geometric dimensions of the probe profile and integrating the mechanical calculations with experimental

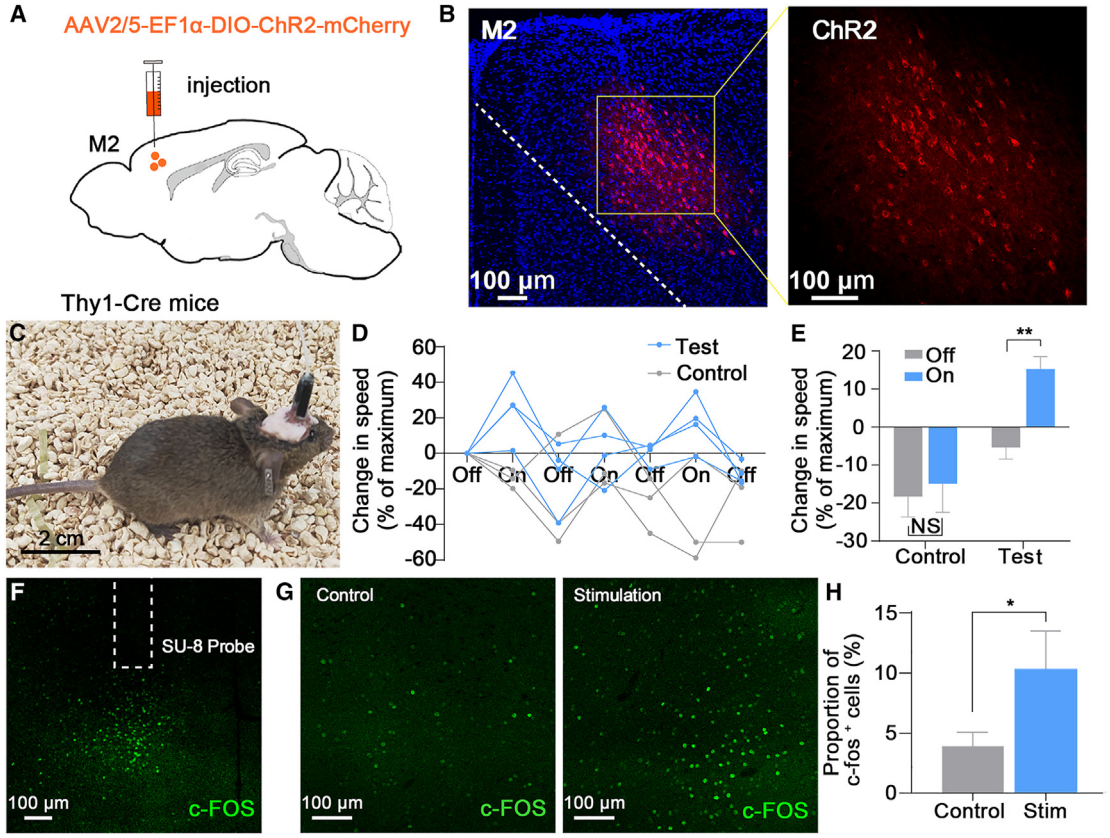

Figure 5. Animal behavior experiment

(A) Illustration of the virus injection.

(B) Imaging of ChR2 photosensitive protein expression (M2) region on the right of the white dotted line (DAPI in blue). Both scale bars, 100 μm.

(C) Photograph of mice recovering from the probe implantation surgery (scale bar, 2 cm).

(D) Motion velocity changes of mice in the control group at 589 nm wavelength and the experimental group at 473 nm wavelength in light and non-light time. $N = 3$ mice in the control group; $N = 4$ mice in the experimental group.

(E) Quantitative statistical comparison chart between the control and the experimental group. In the experimental group, 473 nm of light could induce mice to move faster. Two-way ANOVA (Fisher's least significant difference [LSD] test), $^{**}p < 0.01$. NS is non-significance, meaning that there is no difference between the two groups.

(F) c-Fos-positive cells are predominantly expressed below the flexible waveguide probe implantation area (scale bar, 100 μm).

(G) Confocal images of c-Fos expression in the corresponding region on the 473 nm light stimulation side (stimulation) and the contralateral side (control). Both scale bars, 100 μm.

(H) Quantification of the percentage of c-Fos-positive cells in (G) relative to the NeuN-positive cells in the same field of view. Unpaired t test with $p = 0.0476$.

validation. This model helps to predict the successful and precise implantation of mechanically flexible neural probes. As long as the feature contour information of the flexible probe falls within the implantable range of the model, researchers can implant the flexible probe directly without any additional assistance, which is user friendly for surgical operators. Following the establishment of the implantation model, we present a convenient approach for fabricating flexible waveguide probes made of polymer with low propagation loss and long-term minimal inflammatory responses to brain tissue. Compared to traditional rigid silicon probes, the preparation process of flexible probes involves fewer steps and requires less manufacturing time. Furthermore, the lower bending stiffness of the polymer-based flexible waveguide probes minimizes the relative interaction with the brain tissue, thereby reducing the risk of damage and inflammatory response. The successful modulation of the mouse movement speed using these probes underscores their reliability and

effectiveness in neuroscientific research. Our findings not only address process concerns but also provide valuable insights for the development of flexible optoelectronic optogenetic tools. These advancements hold promise for future applications in neurology science, offering innovative solutions for studying brain functions and behaviors.

Although flexible waveguide probes have demonstrated certain advantages in mitigating tissue reactions and reducing the complexity of implantation surgery, there are several areas that warrant further expansion in terms of functional development and probe application. First, the current coupling and packaging of the probe with optical fibers impose limitations on the range of movement of the mice. The integration of an on-chip diode-pumped laser[32] with a flexible waveguide probe, along with the incorporation of wireless functionality and signal transmission, represents an enhanced approach. Furthermore, although here we mainly focus on the low-trauma characteristics of flexible waveguide probes for brain tissue and solving the problem of difficult implantation of flexible waveguide probes, this platform technology may provide different strategies for the integration of flexible multifunctional waveguide-based optogenetic probes. For instance, by incorporating inorganic waveguide materials into SU-8, high-refractive-index contrast structures[35,36,49,50] can be formed, reducing the device dimensions and achieving a denser integration of multifunctional devices. Finally, more intricate geometric profile structure optimization techniques can be used to further improve the implantation depth of the flexible probe.[51] The progress demonstrated by this work offers valuable insights for designing and developing flexible waveguide probes that producers can efficiently prepare and that are user friendly for surgical operators in future applications. It also holds great potential for long-term experimentation and monitoring of chronic diseases.

EXPERIMENTAL PROCEDURES

Experimental animals in the mechanical analysis, inflammation comparison, and behavioral modulation

All the implantation surgeries of mechanical analysis were performed in two anesthetized 8-week-old C57BL/6 mice, with brain tissue exposed through a cranial window. The implantation experiments of inflammation comparison were performed on 36 male wild-type C57BL/6 mice (8–10 weeks old). The behavioral modulation experiments used four male Thy1-Cre transgenic mice obtained from the Jackson Laboratory (FVB/N-Tg(Thy1-cre)1Vln/J, stock no. 006143). All animal experiments were conducted following the guidelines for the Care and Use of Laboratory Animals of Zhejiang University, which were approved by the Committee for Animal Experiments of Zhejiang University. Other related details are presented in the supplemental information.

RESOURCE AVAILABILITY

Lead contact

Further information and requests for resources should be directed to the lead contact, Lan Li (lilan@westlake.edu.cn).

Materials availability

This study did not generate novel unique materials.

Data and code availability

All data needed to evaluate the conclusions of the study are presented in the paper and supplemental information.

ACKNOWLEDGMENTS

We are grateful for financial support from the Key R&D Program of Zhejiang Province (2024C03150); the National Natural Science Foundation of China (62175202); the Natural Science Foundation of Zhejiang Province (LR22F050007); the Key R&D Program of Zhejiang Province (2024SSYS0031 and 2021C03001); the MOE Frontier Science Center for Brain Science & Brain-Machine Integration, Zhejiang University; the Leading Innovative and Entrepreneur Team Introduction Program of Zhejiang (2020R01005 and 202099144); the CAMS Innovation Fund for Medical Sciences (2019-I2M-5-057); the Special Support Plan for Photoelectric Chips Research at Westlake University (10300000 H062401/001); and the Start-up Fund of Westlake University. The authors would also like to acknowledge the Westlake Center for Micro/Nano Fabrication and Instrumentation, the Service Center for Physical Sciences at Westlake University, and the ZJU Micro-Nano Fabrication Center at Zhejiang University for the facility support. The authors thank Lingxiao Gao for assistance with the bio-experiments.

AUTHOR CONTRIBUTIONS

Z.C., X.L., Y.T., and Z.H. contributed equally to this work. Z.C., X.L., Y.T., Z.H., H.J., K.S., W.G., and L.L. designed the experiments and analyzed the results. Z.C., Y.T., J.H., Y.W., R.T., K.B., J.J., Y. Ye, Y. Yun, and L.W. fabricated the probe and conducted optical performance characterization. X.L. and Y.Z. designed and conducted bio-experiments. Z.C., Y.T., Z.H., J.H., H.L., J.Z., and Z.L. conducted mechanical testing and analysis. H.J., K.S., W.G., and L.L. conceived and supervised the study. All authors discussed the results and wrote the manuscript.

DECLARATION OF INTERESTS

The authors declare no competing interests.

SUPPLEMENTAL INFORMATION

Supplemental information can be found online at https://doi.org/10.1016/j.xcrp.2024.102217.

Received: June 11, 2024
Revised: August 14, 2024
Accepted: August 30, 2024
Published: September 23, 2024

REFERENCES

1. Vázquez-Guardado, A., Yang, Y., Bandodkar, A.J., and Rogers, J.A. (2020). Recent advances in neurotechnologies with broad potential for neuroscience research. Nat. Neurosci. *23*, 1522–1536.

2. Won, S.M., Song, E., Reeder, J.T., and Rogers, J.A. (2020). Emerging modalities and implantable technologies for neuromodulation. Cell *181*, 115–135.

3. Li, H., Wang, J., and Fang, Y. (2023). Recent developments in multifunctional neural probes for simultaneous neural recording and modulation. Microsyst. Nanoeng. *9*, 4. https://doi.org/10.1038/s41378-022-00444-5.

4. Tian, H., Xu, K., Zou, L., and Fang, Y. (2022). Multimodal neural probes for combined optogenetics and electrophysiology. iScience *25*, 103612. https://doi.org/10.1016/j.isci.2021.103612.

5. Chen, H., and Fang, Y. (2023). Recent developments in implantable neural probe technologies. MRS Bull. *48*, 484–494. https://doi.org/10.1557/s43577-023-00535-2.

6. Zhang, F., Wang, L.-P., Brauner, M., Liewald, J.F., Kay, K., Watzke, N., Wood, P.G., Bamberg, E., Nagel, G., Gottschalk, A., and Deisseroth, K. (2007). Multimodal fast optical interrogation of neural circuitry. Nature *446*, 633–639.

7. Li, L., Lu, L., Ren, Y., Tang, G., Zhao, Y., Cai, X., Shi, Z., Ding, H., Liu, C., Cheng, D., et al. (2022). Colocalized, bidirectional optogenetic modulations in freely behaving mice with a wireless dual-color optoelectronic probe. Nat. Commun. *13*, 839.

8. Cai, X., Zhang, H., Wei, P., Liu, Q., Sheng, D., Li, Z., Zhang, B., Tang, G., Zhao, W., Ye, Z., et al. (2024). A wireless optoelectronic probe to monitor oxygenation in deep brain tissue. Nat. Photonics *18*, 492–500.

9. Nazempour, R., Zhang, B., Ye, Z., Yin, L., Lv, X., and Sheng, X. (2022). Emerging applications of optical fiber-based devices for brain research. Adv. Fiber Mater. *4*, 24–42.

10. Pisanello, F., Sileo, L., Oldenburg, I.A., Pisanello, M., Martiradonna, L., Assad, J.A., Sabatini, B.L., and De Vittorio, M. (2014). Multipoint-Emitting Optical Fibers for Spatially Addressable In Vivo Optogenetics. Neuron *82*, 1245–1254. https://doi.org/10.1016/j.neuron.2014.04.041.

11. Holleis, S., Hoinkes, T., Wuttke, C., Schneeweiss, P., and Rauschenbeutel, A. (2014). Experimental stress–strain analysis of tapered silica optical fibers with nanofiber waist. Appl. Phys. Lett. *104*, 163109. https://doi.org/10.1063/1.4873339.

12. Chen, R., Canales, A., and Anikeeva, P. (2017). Neural recording and modulation technologies. Nat. Rev. Mater. *2*, 16093–16116.

13. Axpe, E., Orive, G., Franze, K., and Appel, E.A. (2020). Towards brain-tissue-like biomaterials. Nat. Commun. *11*, 3423.

14. Kim, T.-i., McCall, J.G., Jung, Y.H., Huang, X., Siuda, E.R., Li, Y., Song, J., Song, Y.M., Pao, H.A., Kim, R.-H., et al. (2013). Injectable, cellular-scale optoelectronics with applications for wireless optogenetics. Science *340*, 211–216.

15. Reddy, J.W., Kimukin, I., Stewart, L.T., Ahmed, Z., Barth, A.L., Towe, E., and Chamanzar, M. (2019). High density, double-sided, flexible optoelectronic neural probes with embedded μLEDs. Front. Neurosci. *13*, 455147.

16. Klein, E., Gossler, C., Paul, O., and Ruther, P. (2018). High-density μLED-based optical cochlear implant with improved thermomechanical behavior. Front. Neurosci. *12*, 413393.

17. Yang, Y., Wu, M., Vázquez-Guardado, A., Wegener, A.J., Grajales-Reyes, J.G., Deng, Y., Wang, T., Avila, R., Moreno, J.A., Minkowicz, S., et al. (2021). Wireless multilateral devices for optogenetic studies of individual and social behaviors. Nat. Neurosci. *24*, 1035–1045. https://doi.org/10.1038/s41593-021-00849-x.

18. Lee, S.H., Kim, J., Shin, J.H., Lee, H.E., Kang, I.-S., Gwak, K., Kim, D.-S., Kim, D., and Lee, K.J. (2018). Optogenetic control of body movements via flexible vertical light-emitting diodes on brain surface. Nano Energy *44*,

447–455. https://doi.org/10.1016/j.nanoen.2017.12.011.

19. Cao, Y., Pan, S., Yan, M., Sun, C., Huang, J., Zhong, C., Wang, L., and Yi, L. (2021). Flexible and stretchable polymer optical fibers for chronic brain and vagus nerve optogenetic stimulations in free-behaving animals. BMC Biol. *19*, 252–313.

20. Wang, L., Zhong, C., Ke, D., Ye, F., Tu, J., Wang, L., and Lu, Y. (2018). Ultrasoft and highly stretchable hydrogel optical fibers for in vivo optogenetic modulations. Adv. Opt. Mater. *6*, 1800427.

21. Zhou, Y., Gu, C., Liang, J., Zhang, B., Yang, H., Zhou, Z., Li, M., Sun, L., Tao, T.H., and Wei, X. (2022). A silk-based self-adaptive flexible opto-electro neural probe. Microsyst. Nanoeng. *8*, 118.

22. Fu, R., Luo, W., Nazempour, R., Tan, D., Ding, H., Zhang, K., Yin, L., Guan, J., and Sheng, X. (2018). Implantable and biodegradable poly (l-lactic acid) fibers for optical neural interfaces. Adv. Opt. Mater. *6*, 1700941.

23. Reddy, J.W., Lassiter, M., and Chamanzar, M. (2020). Parylene photonics: a flexible, broadband optical waveguide platform with integrated micromirrors for biointerfaces. Microsyst. Nanoeng. *6*, 85.

24. Liu, X., Rao, S., Chen, W., Felix, K., Ni, J., Sahasrabudhe, A., Lin, S., Wang, Q., Liu, Y., He, Z., et al. (2023). Fatigue-resistant hydrogel optical fibers enable peripheral nerve optogenetics during locomotion. Nat. Methods *20*, 1802–1809. https://doi.org/10.1038/s41592-023-02020-9.

25. Huang, S., Liu, X., Lin, S., Glynn, C., Felix, K., Sahasrabudhe, A., Maley, C., Xu, J., Chen, W., Hong, E., et al. (2024). Control of polymers' amorphous-crystalline transition enables miniaturization and multifunctional integration for hydrogel bioelectronics. Nat. Commun. *15*, 3525. https://doi.org/10.1038/s41467-024-47988-w.

26. Jeong, J.-W., McCall, J.G., Shin, G., Zhang, Y., Al-Hasani, R., Kim, M., Li, S., Sim, J.Y., Jang, K.-I., Shi, Y., et al. (2015). Wireless Optofluidic Systems for Programmable In Vivo Pharmacology and Optogenetics. Cell *162*, 662–674. https://doi.org/10.1016/j.cell.2015.06.058.

27. Andersen, M.A., and Schouenborg, J. (2023). Polydimethylsiloxane as a more biocompatible alternative to glass in optogenetics. Sci. Rep. *13*, 16090. https://doi.org/10.1038/s41598-023-43297-2.

28. Dey, P.K., and Ganguly, P. (2014). A technical report on fabrication of SU-8 optical waveguides. J. Opt. *43*, 79–83.

29. Son, Y., Lee, H.J., Kim, J., Shin, H., Choi, N., Lee, C.J., Yoon, E.-S., Yoon, E., Wise, K.D., Kim, T.G., and Cho, I.J. (2015). In vivo optical modulation of neural signals using monolithically integrated two-dimensional neural probe arrays. Sci. Rep. *5*, 15466.

30. Rubehn, B., Wolff, S.B.E., Tovote, P., Lüthi, A., and Stieglitz, T. (2013). A polymer-based neural microimplant for optogenetic applications: design and first in vivo study. Lab Chip *13*, 579–588. https://doi.org/10.1039/C2LC40874K.

31. Luan, L., Wei, X., Zhao, Z., Siegel, J.J., Potnis, O., Tuppen, C.A., Lin, S., Kazmi, S., Fowler, R.A., Holloway, S., et al. (2017). Ultraflexible nanoelectronic probes form reliable, glial scar–free neural integration. Sci. Adv. *3*, e1601966.

32. Kampasi, K., English, D.F., Seymour, J., Stark, E., McKenzie, S., Vöröslakos, M., Buzsáki, G., Wise, K.D., and Yoon, E. (2018). Dual color optogenetic control of neural populations using low-noise, multishank optoelectrodes. Microsyst. Nanoeng. *4*, 10.

33. Reddy, J.W., and Chamanzar, M. (2018). Low-loss flexible Parylene photonic waveguides for optical implants. Opt. Lett. *43*, 4112–4115.

34. Chen, Y., and Li, M. (2014). Integrated silicon and silicon nitride photonic circuits on flexible substrates. Opt. Lett. *39*, 3449–3452.

35. Chen, Z., Shi, Y., Wei, M., Luo, Y., Ma, H., Tang, R., Weng, Y., Dai, H., Zhong, C., Sun, C., et al. (2023). A universal approach to high-index-contrast flexible integrated photonics. Adv. Opt. Mater. *11*, 2202824.

36. Li, L., Zhang, P., Wang, W.-M., Lin, H., Zerdoum, A.B., Geiger, S.J., Liu, Y., Xiao, N., Zou, Y., Ogbuu, O., et al. (2015). Foldable and cytocompatible sol-gel TiO2 photonics. Sci. Rep. *5*, 13832.

37. Reddy, J.W., Jain, V., Guessaymi, N., Malekoshoaraie, M.H., and Chamanzar, M. (2023). In Vivo Optogenetic Stimulation Using Parylene Photonic Waveguides for Light Delivery, pp. 26–32. (SPIE).

38. Park, S., Yuk, H., Zhao, R., Yim, Y.S., Woldeghebriel, E.W., Kang, J., Canales, A., Fink, Y., Choi, G.B., Zhao, X., and Anikeeva, P. (2021). Adaptive and multifunctional hydrogel hybrid probes for long-term sensing and modulation of neural activity. Nat. Commun. *12*, 3435.

39. Na, K., Sperry, Z.J., Lu, J., Vöröslakos, M., Parizi, S.S., Bruns, T.M., Yoon, E., and Seymour, J.P. (2020). Novel diamond shuttle to deliver flexible neural probe with reduced tissue compression. Microsyst. Nanoeng. *6*, 37. https://doi.org/10.1038/s41378-020-0149-z.

40. Guo, Z., Wang, F., Wang, L., Tu, K., Jiang, C., Xi, Y., Hong, W., Xu, Q., Wang, X., Yang, B., et al. (2022). A flexible neural implant with ultrathin substrate for low-invasive brain–computer interface applications. Microsyst. Nanoeng. *8*, 133. https://doi.org/10.1038/s41378-022-00464-1.

41. Klapoetke, N.C., Murata, Y., Kim, S.S., Pulver, S.R., Birdsey-Benson, A., Cho, Y.K., Morimoto, T.K., Chuong, A.S., Carpenter, E.J., Tian, Z., et al. (2014). Independent optical excitation of distinct neural populations. Nat. Methods *11*, 338–346.

42. MacManus, D.B., Pierrat, B., Murphy, J.G., and Gilchrist, M.D. (2017). Region and species dependent mechanical properties of adolescent and young adult brain tissue. Sci. Rep. *7*, 13729.

43. Chen, Z., and Lee, J.-B. (2021). Biocompatibility of su-8 and its biomedical device applications. Micromachines *12*, 794.

44. Wang, Y., Yang, X., Zhang, X., Wang, Y., and Pei, W. (2023). Implantable intracortical microelectrodes: reviewing the present with a focus on the future. Microsyst. Nanoeng. *9*, 7.

45. Wellman, S.M., and Kozai, T.D.Y. (2017). Understanding the Inflammatory Tissue Reaction to Brain Implants To Improve Neurochemical Sensing Performance. ACS Chem. Neurosci. *8*, 2578–2582. https://doi.org/10.1021/acschemneuro.7b00403.

46. Lee, Y., Shin, H., Lee, D., Choi, S., Cho, I.J., and Seo, J. (2021). A lubricated nonimmunogenic neural probe for acute insertion trauma minimization and long-term signal recording. Adv. Sci. *8*, 2100231.

47. Salatino, J.W., Ludwig, K.A., Kozai, T.D.Y., and Purcell, E.K. (2017). Glial responses to implanted electrodes in the brain. Nat. Biomed. Eng. *1*, 862–877.

48. Montgomery, K.L., Yeh, A.J., Ho, J.S., Tsao, V., Mohan Iyer, S., Grosenick, L., Ferenczi, E.A., Tanabe, Y., Deisseroth, K., Delp, S.L., and Poon, A.S.Y. (2015). Wirelessly powered, fully internal optogenetics for brain, spinal and peripheral circuits in mice. Nat. Methods *12*, 969–974. https://doi.org/10.1038/nmeth.3536.

49. Chen, Z., Wei, M., Luo, Y., Jian, J., Ye, Y., Yin, Y., Sun, C., Zhong, C., Si, K., Zhang, D., et al. (2022). Efficient and compact sol-gel TiO2 thermo-optic microring resonator modulator. Opt. Mater. Express *12*, 4061–4071.

50. Li, L., Lin, H., Qiao, S., Zou, Y., Danto, S., Richardson, K., Musgraves, J.D., Lu, N., and Hu, J. (2014). Integrated flexible chalcogenide glass photonic devices. Nat. Photonics *8*, 643–649.

51. Zou, D., Wang, X., Yang, H., Jiang, W., Zhu, Z., Tao, C., Zhou, Z., Sun, L., Tao, T.H., and Wei, X. (2024). Tea Wing Bug Inspired Flexible Deep Brain Probe Minimally Invasive Implantation (IEEE), pp. 449–452.